Received: 7 June 2023 | Revised: 12 January 2024 | Accepted: 15 January 2024

DOI: 10.1002/mrm.30034

RESEARCH ARTICLE

Magnetic Resonance in Medicine

Investigating apparent differences between standard DKI and axisymmetric DKI and its consequences for biophysical parameter estimates

Jan Malte Oeschger[1] | **Karsten Tabelow**[2] | **Siawoosh Mohammadi**[1,3,4]

[1]Department of Systems Neuroscience, University Medical Center Hamburg-Eppendorf, Hamburg, Germany

[2]Weierstrass Institute for Applied Analysis and Stochastics, Berlin, Germany

[3]Department of Neurophysics, Max Planck Institute for Human Cognitive and Brain Sciences, Leipzig, Sachsen Germany

[4]Max Planck Research Group MR Physics, Max Planck Institute for Human Development, Berlin, Germany

Correspondence
Siawoosh Mohammadi, Max Planck Research Group MR Physics, Max Planck Institute for Human Development, Lentzeallee 94, 14195 Berlin, Germany.
Email: mohammadi@mpib-berlin.mpg.de

Funding information
Bundesministerium für Bildung und Forschung, Grant/Award Numbers: 01EW1711A, 01EW1711B; Deutsche Forschungsgemeinschaft, Grant/Award Numbers: MO 2397/5-1, MO 2397/5-2; Deutsche Forschungsgemeinschaft, Grant/Award Numbers: MO 2397/4-1, MO 2397/4-2

Abstract

Purpose: The purpose of the study is to identify differences between axisymmetric diffusion kurtosis imaging (DKI) and standard DKI, their consequences for biophysical parameter estimates, and the protocol choice influence on parameter estimation.

Methods: Noise-free and noisy, synthetic diffusion MRI human brain data is simulated using standard DKI for a standard and the fast "199" acquisition protocol. First the noise-free "baseline" difference between both DKI models is estimated and the influence of fiber complexity is investigated. Noisy data is used to establish the signal-to-noise ratio at which the baseline difference exceeds noise variability. The influence of protocol choices and denoising is investigated. The five axisymmetric DKI tensor metrics (AxTM), the parallel and perpendicular diffusivity and kurtosis and mean of the kurtosis tensor are used to compare both DKI models. Additionally, the baseline difference is also estimated for the five parameters of the WMTI-Watson model.

Results: The parallel and perpendicular kurtosis and all of the WMTI–Watson parameters had large baseline differences. Using a Westin or FA mask reduced the number of voxels with large baseline difference, that is, by selecting voxels with less complex fibers. For the noisy data, precision was worsened by the fast "199" protocol but adaptive denoising can help counteract these effects.

Conclusion: For the diffusivities and mean of the kurtosis tensor, axisymmetric DKI with a standard protocol delivers similar results as standard DKI. Fiber complexity is one main driver of the baseline differences. Using the "199" protocol worsens precision in noisy data but adaptive denoising mitigates these effects.

KEYWORDS

apparent differences, axisymmetric DKI, bias, biophysical parameters, standard DKI, white matter

1 | INTRODUCTION

Diffusion kurtosis imaging (DKI) has increasingly been used to study the neuronal tissue microstructure and derive biophysical parameters relevant for understanding brain function and impact of disease[1–3] during the past ten years. DKI is a more complex extension of the diffusion tensor imaging (DTI) framework and provides diffusion kurtosis metrics that can provide complementary information[4–6] to DTI. However, the increased complexity comes with an increase in acquisition time. Since time is a limited resource in scientific and especially clinical settings, needing more time poses a major hurdle for a more extensive implementation and application of DKI.

Axisymmetric DKI was recently introduced as a more acquisition time efficient DKI model.[7–9] Axisymmetric DKI reduces the parameter space by imposing additional symmetry assumptions, that is, axisymmetrically organized fibers in the imaged tissue structure and axisymmetric DKI (eight parameters) can be fitted with less data than is required by standard DKI (22 parameters). One time-efficient acquisition scheme that leverages axisymmetric DKI's data demand advantages is the fast "199" scheme[7,10] that relies on a total of 19 images (18 diffusion weighted images and one nondiffusion weighted image), only. However, parameter estimation from fewer diffusion weighted images is more susceptible to noise and it can be expected that the signal-to-noise ratio (SNR) requirements for accurate parameter estimates are higher when fitting data acquired with the fast "199" protocol compared to a standard diffusion MRI (dMRI) protocol. To mitigate the influence of noise, denoising algorithms can be used.[11,12]

An important parameter subset existing in both axisymmetric DKI and standard DKI are the five axisymmetric DKI tensor metrics (AxTM), the parallel and perpendicular diffusivity ($D_{\parallel}$ and $D_{\perp}$) and kurtosis ($W_{\parallel}$ and $W_{\perp}$) and mean of the kurtosis tensor ($\overline{W}$). Since the AxTM are attainable with both DKI models, they are perfectly suited to be used for a model comparison. The five AxTM are also directly related to the five parameters of the biophysical standard model,[13] the axon water fraction AWF, axon dispersion κ, parallel and perpendicular extra-axonal diffusivities $D_{e,\parallel}$ and $D_{e,\perp}$ and intra axonal diffusivity D_a, here estimated with the WMTI–Watson model.[14,15]

It has been suggested that the symmetry assumptions made in axisymmetric DKI are likely a reasonable approximation to diffusion in major white matter fiber bundles, for example, occurring in white matter.[7] Violation of these additional symmetry assumptions, for example, in white matter voxels containing crossing fibers, might lead to a deviation of axisymmetric DKI fit results from their standard DKI reference counterpart.

In this work, we simulate synthetic white matter data using standard DKI as forward model to explicitly include complex, non-axisymmetric fiber configurations. We hypothesize that any observed deviation between both DKI model variants is due to an error in axisymmetric DKI rooted in an underlying complex and thus non-axisymmetric fiber configuration. To test this hypothesis, voxel selection masks are used to filter out voxels with high fiber complexity that likely break axisymmetric DKI's symmetry assumptions. Furthermore, we establish the "baseline difference" between axisymmetric DKI and standard DKI AxTM estimates from noise-free data. The baseline differences are inherent to axisymmetric DKI and will always be there with respect to standard DKI. Another topic is the influence of noise on the standard deviation (SD) of axisymmetric DKI fit results. Here the question at which SNR the baseline difference between both DKI models becomes bigger than axisymmetric DKI's SD is investigated. This will establish an SNR regime where the standard deviation caused by noise dominates parameter estimation and at what SNR the baseline difference between both DKI models becomes visible which is here referred to as the "tipping point". To investigate this, first a noise simulation study is performed where the SNR space is densely sampled to precisely establish the tipping point without using denoising methods. Then, we use Multi-shell Position-Orientation Adaptive Smoothing (msPOAS), an adaptive denoising algorithm that is preserving tissue boundaries without introducing blurring[11,16,17] to establish if the tipping point can be reached for realistic SNRs in voxels where the axisymmetric conditions were best fulfilled. In both noise studies, the influence of the acquisition protocol (fast "199" protocol vs. a standard dMRI protocol) is investigated as an additional variable. Finally, the median bias based on the two acquisition protocols is quantified in five well known fiber tracts for a typical SNR found in dMRI datasets.[18] Throughout the work, the noise-free estimates of the five AxTM or the biophysical parameters based on standard DKI are used as a ground truth reference and axisymmetric DKI fit results are compared to them on a voxel-wise basis, hence the baseline difference between axisymmetric DKI and standard DKI is also referred to as "bias".

2 | METHODS

A detailed description of the standard DKI model and the axisymmetric DKI model is provided in the Sections S1.1 and S1.2 but can also be found in References 7 and 19.

2.1 | Dataset

2.1.1 | Acquisition

Multishell, in vivo dMRI data with 153 diffusion gradient directions and b-values of 0 s/mm^2 (18 images), 550 s/mm^2 (30 directions), 1100 s/mm^2 (45 directions), and 2500 s/mm^2 (60 directions) $\frac{\text{s}}{\text{mm}^2}$ was acquired from a healthy volunteer at 3T with: FOV of $200 \times 203 \times 170\,\text{mm}^3$ at 1.7 mm isotropic resolution, TE = 75 ms, TR= 5800 ms, gradient separation $\Delta = 38.8$ ms and gradient pulse duration $\delta = 13.3$ ms. Image reconstruction at the scanner from the multichannel information was done using a sum of squares algorithm where all channels had the same weights. The following pre-processing was applied to the dMRI data using the ACID toolbox[20] (in that order): eddy current and motion artifact correction using the ACID "ECMOCO" module, susceptibility artifact correction using the ACID "HySCO" module and Rician bias correction using the ACID "Rician bias correction" module that uses a second moment approach and acts on the signals of the individual diffusion weighted images as described in Reference 21. The noise level σ was calculated using the ACID "Noise estimation" module with the "repeated measures" method where σ is estimated as the averaged SD over the diffusion measurements of the highest diffusion shell in the ventricles, see Reference 20. Additionally, we acquired multiparameter mapping data[22] on the same subject and calculated the R_1 map using the hMRI toolbox,[23] for anatomical visualization.

The in vivo dMRI data used for this study was acquired with the help of a human research participant. The participant provided written informed consent. The local ethics committees at University Medical Center Hamburg-Eppendorf approved the study (PV5141).

2.1.2 | Generation of synthetic data

The acquired multishell, in vivo dMRI data was fitted with standard DKI to obtain the 22 standard DKI tensor metrics per voxel which were then used for generation of noise-free, synthetic dMRI data using standard DKI as a forward model with the same diffusion shells and gradient directions that were used to acquire the data.

2.2 | Biophysical parameters

The framework presented in Reference 13, here referred to as "WMTI-Watson," was used to establish an analytical connection between the five AxTM $\Omega = \{\overline{W}, W_{\parallel}, W_{\perp}, D_{\parallel}, D_{\perp}\}$ and the biophysical parameters $\beta = \{\text{AWF}, \kappa, D_{e,\perp}, D_{e,\parallel}, D_a\}$. A detailed description of the framework can be found in Section S1.3.

We neglected a potential model error of the WMTI–Watson model with respect to the biological tissue ground truth and assumed the biophysical parameters based on AxTM estimates from standard DKI to be the ground truth. In this study, we focused on quantifying the propagation of the error in the AxTM estimates into the respective WMTI–Watson parameter estimates introduced by axisymmetric DKI.

2.3 | Computation of difference between both DKI models and substantially differing voxels

The estimated parameters, either the set of AxTM Ω or the set of biophysical parameters β were estimated based on standard DKI and axisymmetric DKI and compared using the voxel-wise absolute percentage error (A-PE):

$$\text{A-PE} = 100 \cdot \frac{|\theta_{standardDKI} - \theta_{\text{axisymmetricDKI}}|}{\theta_{standardDKI}} \qquad (1)$$

Here θ is an element of either Ω or β and the subscript indicates whether the parameter was estimated based on standard DKI or axisymmetric DKI. If A-PE > 5%, the corresponding voxel was classified as a "substantially differing voxel" (SDV). The study focused on white matter only, to obtain the white matter mask, we segmented the R_1 map into tissue probability maps (TPM) and thresholded the white matter TPM (TPM > 0.9), see green contour in Figure 2. To summarize the results we estimated a) the number of SDV in white matter in percent and b) the median A-PE in the population of SDV. We implemented the condition $\theta \in \Omega \geq 0$ and $\theta \in \beta \geq 0$ because negative diffusivities are non-physical and AWF and κ are ≥ 0 by definition. Furthermore, kurtosis estimates in the healthy brain have been found[24] well above 0.

2.3.1 | Influence of voxel selection masks on number of substantially differing voxels

To identify voxels in white matter that likely brake the axisymmetric tissue symmetry assumption,[25,26] two different masks were used: a fractional anisotropy (FA) mask and a so-called "Westin mask." To generate the FA mask, white matter voxels with FA ≥ 0.55 were selected based on the FA of an unidirectional phantom, see Reference 27. This voxel selection is referred to as "FA mask." To generate the Westin mask, white matter voxels that fulfill the conditions imposed by a threshold for the Westin indices computed via the diffusion tensor eigenvalues λ, $C_L = \frac{\lambda_1 - \lambda_2}{\lambda_1} \geq 0.4$, $C_P = \frac{\lambda_2 - \lambda_3}{\lambda_1} \leq 0.2$ and $C_S = \frac{\lambda_3}{\lambda_1} \leq 0.35$[26] were

investigated, this voxel selection is referred to as "Westin mask." For comparison, a third mask containing the entire white matter was used.

2.4 | Noise simulations

2.4.1 | Simulation of noisy dMRI data and fast "199" protocol

The noise-free, in vivo human brain data $\tilde{S}_{\text{noise-free}}$ were noise contaminated according to $S_{\text{cont}} = |\tilde{S}_{\text{noise-free}} + \alpha + \beta i|$, where $\alpha, \beta \in \mathcal{N}(0, \sigma)$ were drawn from a zero mean Gaussian with SD σ. A special property of axisymmetric DKI is that due to it's reduced parameter space, it needs fewer measurements and—at a minimum—all five AxTM can be estimated from a fast two shell setup with nine distinct gradient directions $n^{(i+/-)}$[7,10] and one additional $b = 0$ measurement. Here, the fast protocol was simulated for bvalues of $b = 1100 \frac{s}{mm}$ and $b = 2500 \frac{s}{mm}$.

2.4.2 | Single voxel analysis

Here we asked: at what SNR is the baseline difference between standard DKI and axisymmetric DKI bigger than the SD of axisymmetric DKI? The SNR at which this happens is referred to as "tipping point." To investigate this, we simulated 12 single voxels (see Section S1.7) selected from the white matter of the in vivo human brain data set for densely sampled SNRs = [1, 2, 3, ...140] according to the procedure reported above for 2500 noise samples for the standard MRI protocol described in Section 2.1 and additionally for the fast "199" protocol.[7,10] Then, axisymmetric DKI was fitted to the simulated data. To evaluate the simulation and make it comparable to the noise-free study regarding the SDV, the differences between standard DKI and axisymmetric DKI were normalized to the corresponding average AxTM values in white matter and expressed as a percentage thereof.

2.4.3 | White matter Westin mask analysis with adaptive denoising

To investigate whether the tipping point can be reached for typical SNRs of published DKI protocols, we performed another noise simulation study that used the adaptive denoising "msPOAS" module of the ACID toolbox with two set-ups for the adaptation parameter λ, $\lambda = 10$ and $\lambda = 100$ on noisy, whole brain simulation data. The adaptation bandwidth λ controls the adaptivity of msPOAS,[11] ranging from $\lambda = 0$ (complete adaptation) where the original image is unchanged, to $\lambda = \infty$ (non-adaptive denoising) similar to, for example, Gaussian smoothing. Smoothing was performed in the white matter mask because msPOAS needs coherent regions to work properly, while parameter estimation was done in the Westin mask. For the simulated SNRs, values of published protocols were chosen: SNR = [5, 15, 30, 52] (SNR: 52, see Reference 28, SNRs: 30, 15, 5, see Reference 29) and SNR 100. That data was then fitted with axisymmetric DKI in the Westin mask (see Section 2.3), since the Westin mask turned out to be most effective in reducing the number of SDV (see Section 3.2). To evaluate this analysis, $n = 100$ noise samples were simulated, the SD per voxel was calculated and the median was computed. Second, the percentage of voxels reaching the tipping point was calculated.

2.4.4 | Quantification of bias in fiber tracts

To quantify the difference between both DKI models based on the two acquisition protocols under realistic conditions, the whole brain human dMRI data was simulated and fitted with the fast "199" and the standard acquisition protocol for SNR = 39, which was the SNR reported in one of the original fast "199" protocol studies.[18] Data were smoothed using msPOAS and $\lambda = 100$. "Bias" in this context refers to the difference of the noisy, voxel-wise fit results to the ground truth (noise-free, standard DKI fit results), again computed as the A-PE, see Equation (1). Results were evaluated with a specific focus on five well-known fiber tracts: corpus callosum (cc), superior corona radiata (scr), external capsule (exc), superior longitudinal fasciculus (slf), and posterior corona radiata (pcr). The fiber tracts were identified with the JHU-ICBM-DTI-81 white matter atlas[30] for which it was nonlinearly registered to the subject space of the in vivo dMRI data using the spatial normalization tool in SPM12, see Figure 1.

3 | RESULTS

3.1 | Summary measures: Number of SDV highly parameter dependent and biophysical parameters affected the most. Median A-PE similar across all parameters

3.1.1 | Differences between AxTM across the white matter using the two DKI models

Figure 2 shows the spatial distribution of SDV (see Section 2.3) as red dotted voxels in a slice of the AxTM and biophysical parameters, Figure 3 summarizes the

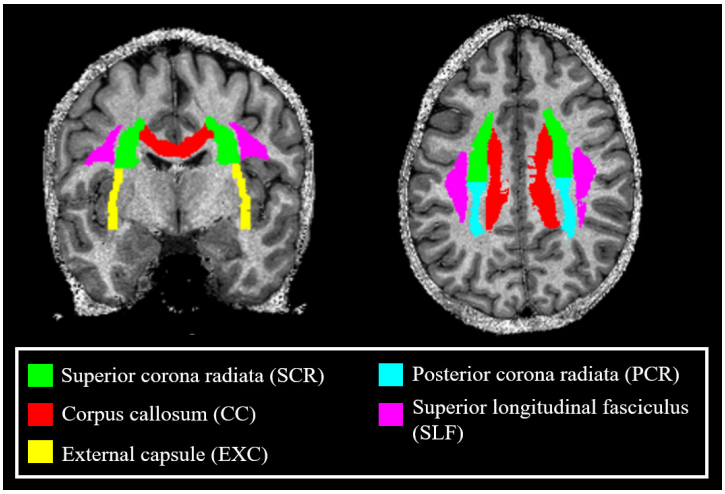

FIGURE 1 The five regions of interest corpus callosum (cc), superior corona radiata (scr), external capsule (exc), superior longitudinal fasciculus (slf) and posterior corona radiata (pcr) identified with the JHU-ICBM-DTI-81 white matter atlas indicated in the coregistered R_1 image of the human brain in vivo dataset used in this study.

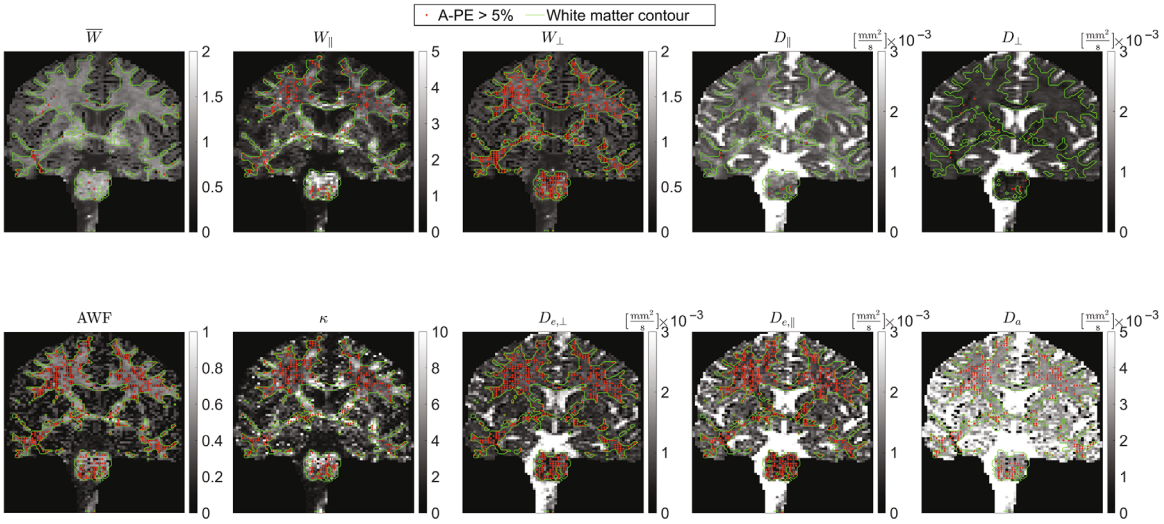

FIGURE 2 Examples of the axisymmetric DKI tensor metrics (top) and biophysical parameters (bottom) in a slice of the human brain data used in this study. The green contour outlines the white matter, the red dots indicate voxels where the A-PE $\geq$ 5% ("substantially differing voxels"). The red barplots of the top row in Figure 3 quantify the percentage of substantially differing voxels in the whole white matter.

number of SDV and the median A-PE in that population using barplots.

The number of SDV in the white matter mask is highly parameter dependent (Figure 3A.1), for example, only 1% of $D_\parallel, D_\perp$ and 2% of the mean of the kurtosis tensor $\overline{W}$. The $W_\parallel$ (22%) and $W_\perp$ (51%) were affected much more, see also spatial distribution of SDV. However, the median difference in the SDV across the AxTM was more similar and ranged between 7% ($\overline{W}$) and 11% ($W_\perp$).

3.1.2 | Differences between biophysical parameters across the white matter based on the two DKI models

Both the number of SDV and the median A-PE in the SDV population (11%–18%) was higher for the biophysical parameters than the AxTM. Again, the percentage of SDV was parameter dependent and spanned from 28% (D_a) to 54% ($D_{e,\parallel}$), see Figure 3B.1. $D_{e,\parallel}$, $D_{e,\perp}$ and AWF had most SDV while D_a and κ had the least. Figure S1 in Section S1.4 documents the underlying A-PE histogram distributions.

For neither the AxTM nor the biophysical parameters Figure 2 revealed a spatial distribution pattern of the SDV in the depicted white matter slice.

3.2 | Influence of voxel selection mask on number of SDV and median bias

Confining the analysis to white matter voxels in the Westin mask reduces the number of SDV more than confining the analysis to white matter voxels in the FA mask. For the AxTM, the median bias remained approximately the same

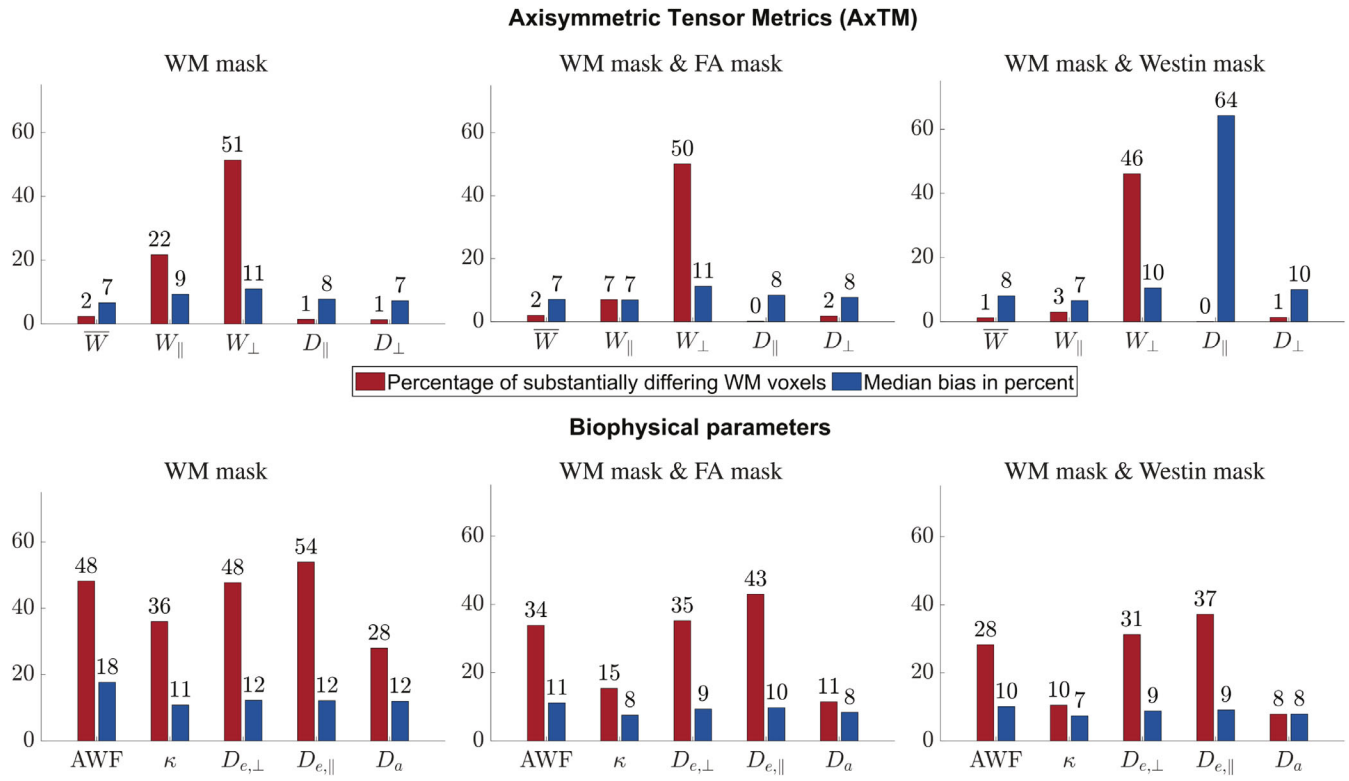

FIGURE 3 Barplots summarizing the number of substantially differing voxels (SDV) of the axisymmetric DKI tensor metrics (AxTM) (top) and biophysical parameters (bottom). Shown is the rounded number of SDV (red barplots) and the median absolute percentage error (A-PE) or "bias" in those voxels (blue barplots). The subplot's titles indicate the subset of voxels that were analyzed, that is, (A.1, B.1) "WM mask" = white matter voxels were analyzed, (A.2, B.2) "WM mask & FA mask" = white matter voxels in the FA mask were analyzed and (A.3, B.3) "WM mask & Westin mask" = white matter voxels in the Westin mask were analyzed. Number of voxels in the white matter mask: 101 521, number of voxels in the WM mask & FA mask analysis: 28 741, number of voxels in the WM mask & Westin mask analysis: 20 527.

for all three voxel masks, except for $D_{\parallel}$ in the Westin mask analysis that was heavily affected by very few outliers with high median bias (64%), while in the case of the biophysical parameters the Westin mask and FA mask could reduce the median bias.

3.2.1 | AxTM

Both, the FA mask and the Westin mask, reduced the number of SDV for all AxTM, compare Figure 3A.2 and A.3. They were most effective for $W_{\parallel}$ and least effective for $W_{\perp}$. For example, for $W_{\perp}$ the number of SDV could be reduced from 51% in the whole white matter to 46% in the Westin mask while for $W_{\parallel}$ the number of SDV could be reduced from 22% to 3%. In general, the Westin mask was more effective in reducing the SDV than the FA mask. Interestingly, the spread of the median A-PE remained similar between ≈7% to ≈11% when applying both masks, see Figure 3A.2, 3A.3, except for $D_{\parallel}$ in the Westin mask that was affected by outliers.

3.2.2 | Biophysical parameters

The same trend as for the AxTM was also observed for the biophysical parameters with regards to the number of SDV: both masks reduced the number of SDV in all parameters significantly and the Westin mask was more effective than the FA mask. But, as opposed to the AxTM, the spread of the median A-PE was also reduced from (11%–18%) to (8%–10%) for the Westin mask and (8%–11%) for the FA mask, see Figure 3B.2,B.3.

3.3 | Noise simulations

3.3.1 | Single voxel analysis

Figure 4 shows the SNR of the tipping point for each of the 12 simulated voxels.The term "bias" here refers to the normalized difference between standard DKI and axisymmetric DKI in %.

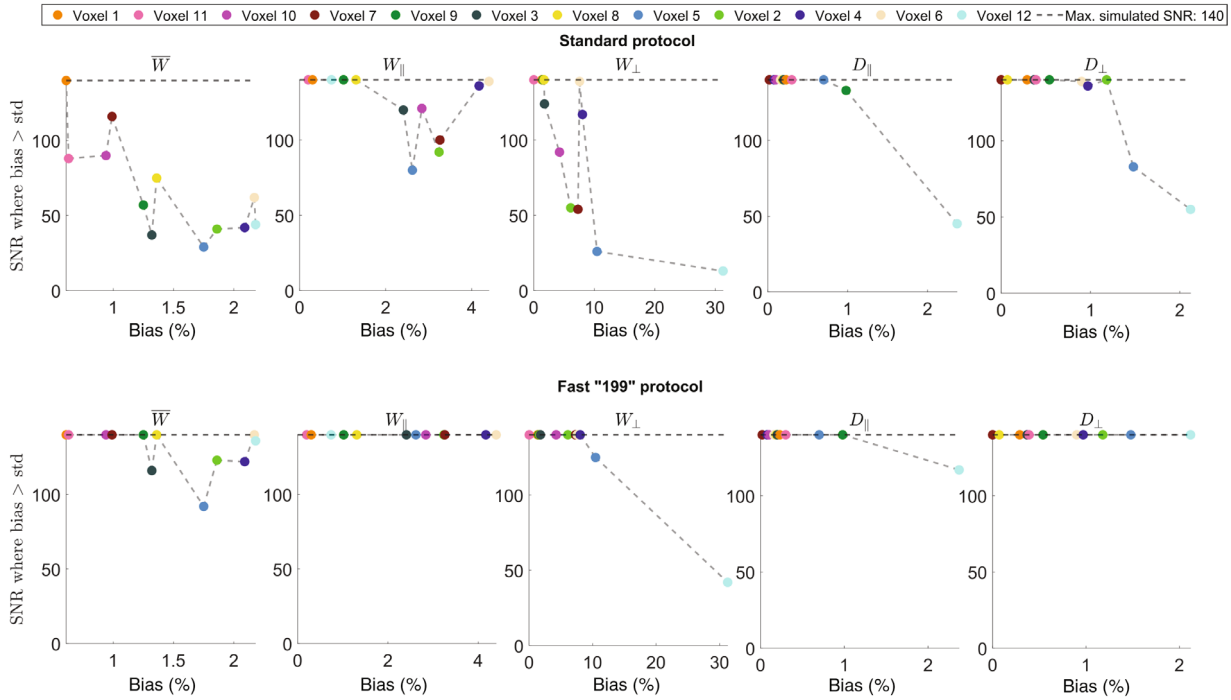

FIGURE 4 Signal-to-noise ratio (SNR) at which the tipping point (bias > std) is reached, computed for $n = 2500$ noise realizations for the 12 simulated voxels. Top shows the results for the standard diffusion kurtosis imaging (DKI) protocol, the bottom shows the results for the fast "199" protocol. The connecting gray line's purpose is to indicate the trend that for higher biases the SNR required to reach the tipping point tends to be lower.

3.3.2 | Standard protocol

The likelihood of finding an SNR threshold ≤140 increases for increasing axisymmetric DKI biases, that is, from left to right on the x-axis. $W_\perp$ and $\overline{W}$ had the highest number of voxels for which a tipping point below the simulation limit (SNR 140) could be found, where the lowest tipping point was found at SNR = 13 for the $W_\perp$ voxel with the highest bias (voxel 12). For the diffusion parameters $D_\perp$ and $D_\parallel$, most voxels did not reach the tipping point up to SNRs = 140.

3.3.3 | Fast "199" protocol

For the fast "199" protocol, too, the likelihood of finding an SNR tipping point ≤140 increases for increasing biases. However, much fewer voxels reached the tipping point below the simulation limit compared to the standard protocol. Again the lowest tipping point was found for the $W_\perp$ voxel with the highest bias (voxel 12).

3.3.4 | White matter Westin mask analysis with adaptive denoising

Figure 5 shows the median SD in the Westin mask (blue and cyan markers), the median difference between standard DKI and axisymmetric DKI in the Westin mask (dashed black line) and the percentage of voxels crossing the voxel-wise tipping point (red and magenta markers, right y-axis).

3.3.5 | Standard protocol

The voxel-wise tipping point was reached for realistic, higher SNRs up to 52 predominantly for the kurtosis parameters but the percentage depended on the adaptation parameter λ. For example, for $\overline{W}$ at SNR = 52, ≈ 37% of voxels reached the tipping point for $\lambda = 100$ while it was only ≈ 14% for $\lambda = 10$. A similar pattern was observed for $W_\perp$ where for SNR = 52, ≈ 28% of voxels reached the tipping point for $\lambda = 100$ and only ≈ 19% in case of $\lambda = 10$. For $W_\parallel$ at SNR = 52 the number of voxels reaching the tipping point was ≈ 7% for $\lambda = 100$ and below 5% for $\lambda = 10$. For the diffusion parameters the number of voxels was close to zero for all realistic SNRs up to 52.

3.3.6 | Fast "199" protocol

The number of voxels reaching the tipping point was lower when the fast protocol was used compared to the standard protocol. For SNR= 52 and $\lambda = 100$ the tipping point was

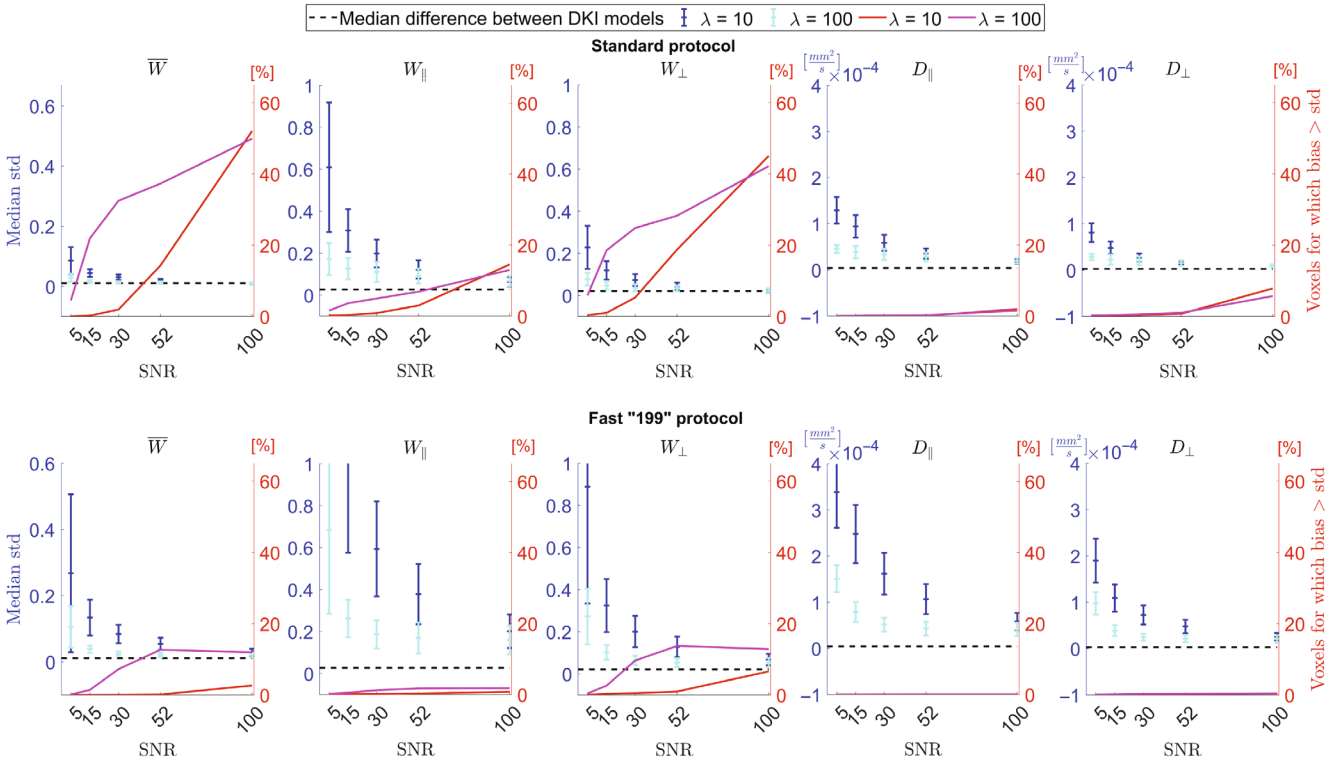

FIGURE 5 Median SD in subset of white matter voxels in Westin mask, computed for n = 100 noise samples (blue and cyan datapoints, left y-axis), median difference between standard diffusion kurtosis imaging (DKI) and axisymmetric DKI in that subsample of voxels (dashed black line) and percentage of voxels crossing the voxel-wise tipping point (red and magenta data, right y-axis). Shown are the results when fitting the standard MRI protocol (top) and the fast "199" protocol (bottom) data, see Sections 2.1 and 2.4.

reached by ≈ 13% of voxels in case of $\overline{W}$ and ≈ 14% in case of $W_\perp$. For SNRs up to 52 and in case of $\lambda = 10$ the number of voxels reaching the tipping point was always close to zero for all parameters.

3.3.7 | Median SD

Independent of the protocol, the median SD always became smaller for increasing SNRs and was also smaller for a higher adaptation parameter λ.

3.3.8 | Quantification of bias in fiber tracts

Figure 6 shows the median bias computed in the five fiber tracts corpus callosum (cc), superior corona radiata (scr), external capsule (exc), superior longitudinal fasciculus (slf), and posterior corona radiata (pcr). The median bias of standard DKI and axisymmetric DKI is always very similar when a standard MRI protocol is used. For $\overline{W}$ the combination of the fast protocol and axisymmetric DKI performs very similarly to when a standard protocol is used while for the other parameters it performs worse.

4 | DISCUSSION

In this work, we found that depending on the parameter, there is a significant number of voxels where axisymmetric DKI and standard DKI inherently differ more than 5%. For $D_\parallel$, $D_\perp$ and $\overline{W}$ we found little differences between the two DKI models, while $W_\perp$ and $W_\parallel$ showed larger differences. All five axisymmetric DKI based biophysical parameters were strongly different from their standard DKI based counterparts. Introduction of two voxel selection masks that reduced the number of voxels containing more complex fiber configurations mitigated the observed differences between both DKI models (especially for $W_\parallel$ and the biophysical parameters) suggesting that fiber complexity is one cause of the observed baseline differences between both DKI models. The noise simulations revealed the challenges of the fast "199" protocol. For a higher but still realistic SNR of 52, the single voxel noise simulation without denoising showed that the baseline differences between axisymmetric DKI and standard DKI are often invisible when a standard MRI acquisition protocol is used (the most tipping points were reached for $\overline{W}$: 5/12 voxels, that is, ≈ 42% and $W_\perp$: 2/12 voxels, that is, ≈ 17%) and that they are almost always invisible when the fast "199" protocol is used (only 1/12 voxels for $W_\perp$ reached the

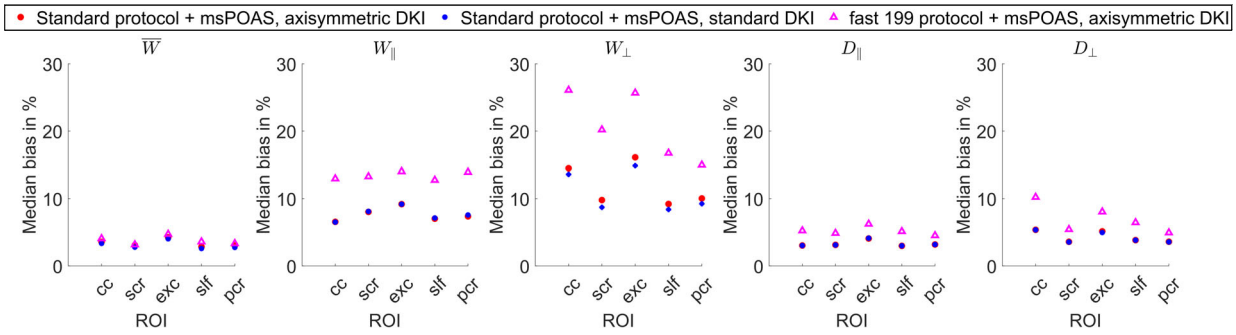

FIGURE 6 Median bias for noisy human brain data at a signal-to-noise ratio (SNR) = 39, smoothed with multi-shell position-orientation adaptive Smoothing (msPOAS) using $\lambda = 100$ in the five white matter fiber tracts corpus callosum (cc), superior corona radiata (scr), external capsule (exc), superior longitudinal fasciculus (slf) and posterior corona radiata (pcr). The median bias was computed for a simulation of the standard protocol that was fitted with standard diffusion kurtosis imaging (DKI) (blue data points) and axisymmetric DKI (red data points) and for a simulation of the fast "199" protocol that was fitted with axisymmetric DKI (pink data points).

tipping point, that is, ≈ 8%). We also found that the SNR of the tipping point depended on the absolute value of the bias. However, in another noise simulation, adaptive denoising improved axisymmetric DKI parameter estimation from the fast protocol to a point where ≈ 13% of $\overline{W}$ voxels and ≈ 14% $W_\perp$ voxels reached the tipping point for realistic SNRs while it did not substantially improve estimation from the standard protocol. Furthermore, our fiber tract analysis revealed that under realistic experimental conditions (realistic SNR and one repeated measurement only), the combination of the fast protocol with adaptive denoising performed similar to standard protocol estimates for $\overline{W}$.

4.1 | Noise-free simulation: baseline differences between AxTM across the white matter using the two DKI models

The AxTM capture different properties of diffusion in tissue and it is not surprising that the observed differences between both DKI models is AxTM dependent. We used the number of SDV to quantify the baseline differences between axisymmetric DKI and standard DKI. We found that the diffusion parameters $D_\parallel$ and $D_\perp$ and the mean of the kurtosis tensor $\overline{W}$ have very few SDV compared to $W_\parallel$ and $W_\perp$.

With a median A-PE of 7%–11% in white matter, the error made in axisymmetric DKI might be acceptable depending on the application. Purely judging from the number of SDV, the diffusion parameters were "safest" where only 1% of white matter voxels were SDV, followed by the mean of the kurtosis tensor $\overline{W}$ with 2%. It can generally be expected that the kurtosis parameters are more sensitive to a model error since they are quadratic in the *b*-value b compared to the linear diffusion parameter counterparts. The propagation of error when fitting the axisymmetric DKI model to dMRI data therefore will be more severe for the kurtosis parameters. Interestingly, the number of SDV increases tenfold from $\overline{W}$ to $W_\parallel$ and roughly doubles from $W_\parallel$ to $W_\perp$. The reason for this trend still needs to be explored.

4.2 | Noise-free simulation: differences between biophysical parameters across the white matter based on the two DKI models

The number of SDV were significantly enhanced in the biophysical parameters (in case of the whole white matter mask up to 54%, see Figure 3) compared to the AxTM from which they were computed. A reason for the enhancement might be that all five AxTM are required to estimate the biophysical parameters, see Section S1.3, and that the connection is complex and nonlinear. The observed AxTM differences could therefore be amplified due to nonlinear effects but also synergistically enhance the number of SDV in the biophysical parameters. However, the found median A-PE of 11%–18% might be acceptable depending on the study.

Also, similar to Reference 31, here the "–" branch tended to yield physically unfeasible, constant high (50) κ values where the objective function did not have a well defined minimum for κ. Furthermore, for this branch $D_{e,\parallel} > D_a$ which in healthy white matter was found to be the biologically invalid solution by most studies.[32] We therefore did not report the results of the – branch.

4.3 | Noise-free simulation: influence of voxel selection mask on number of SDV

The difference between standard DKI and axisymmetric DKI is likely linked to fiber complexity that brakes the symmetry assumptions of axisymmetric DKI. Reducing the

number of voxels with complex fiber structures using voxel selection masks reduced the number of SDV.

The Westin mask reduced the number of SDV in both the AxTM and the biophysical parameters, supporting the hypothesis that differences between both DKI models are linked to the underlying fiber complexity. However, the Westin mask effectiveness was parameter dependent and, for example, worked particularly well for $W_{\parallel}$ where it more than quartered the number of SDV while it had much smaller effects on $W_{\perp}$. The FA mask performed very similarly but reduced the number of SDV slightly less than the Westin mask. In particular, both masks struggled with reducing the number of SDV of $W_{\perp}$.

These findings indicate that next to fiber complexity other factors may play a role in determining the difference between axisymmetric DKI and standard DKI estimates. Other factors that could play a role are differences in glia-cell density,[33] the axonal diameters distribution or the fiber dispersion. With regards to the FA, for example, in vivo tissue FA could also be influenced by factors like the degree of myelination or axon density. This means that the conclusion "if FA ≥ 0.55 then the voxel has a unidirectional fiber configuration" is not necessarily strictly true and voxels in the FA mask might still have a complex fiber structure. The smaller effectiveness of both the FA mask and the Westin mask on $W_{\perp}$ could originate from axisymmetric DKI generally oversimplifying estimation of $W_{\perp}$ since it is directly estimated as one model parameter instead of calculated from three separate tensor metrics as in standard DKI, see, for example, Reference 34.

4.4 | Inter-dependence of A-PE and difference in main fiber orientation

It was shown that axisymmetric DKI produces the same results as standard DKI if two requirements[35] are met, see Section S1.6. Fulfillment of condition b) was not explicitly checked in Reference 35 where differences between axisymmetric DKI and standard DKI were reported. The degree to which the main fiber orientations, estimated with both DKI models, differ can be quantified with the angle ϕ between them. The majority of angles ϕ were between ≈ 1 and 5 degrees in white matter (Figure S3) demonstrating that condition b) is not fulfilled in most cases. Investigating the dependency of the A-PE on angle ϕ using density scatter plots showed an inter-dependency predominantly for $W_{\perp}$ and $W_{\parallel}$, Figure S3. For these parameters these findings indicate that at least to some extent, there is a causal relationship between ϕ and the A-PE.

It could be ruled out that the observed differences between both DKI models in this study is only due to violating condition a) of Reference 35 by implementing a log-of-signals fit demonstrating that this fit implementation still produced different fit results for both DKI models, see Section S1.5.

4.5 | Noise simulations

4.5.1 | Single voxel analysis

Simulating 12 single voxels for $n = 2500$ noise realizations revealed that the tipping point at which the axisymmetric DKI inherent bias is larger than the SD of the axisymmetric DKI parameter estimates was only reached for high, unrealistic SNRs ≥ 52 in most cases. Therefore, the differences between both DKI models will likely not be visible under realistic experimental conditions if techniques like denoising are not used. We found that the tipping point depended on the axisymmetric DKI bias with the strong tendency that the higher the bias, the earlier the tipping point is reached. Furthermore and in line with the main findings that were dealing with the number of SDV per AxTM, it was harder to find the tipping point for the diffusion parameters than the kurtosis parameters, most likely because the diffusion parameters were less biased than the kurtosis parameters and therefore the requirements for the SD to reach the tipping point were too high.

4.5.2 | White matter Westin mask analysis with adaptive denoising

Intuitively one would expect axisymmetric DKI to have better precision than standard DKI because of it's reduced parameter space compared to standard DKI. However, in an earlier study performed on simulations of noisy dMRI data[19] we have found that axisymmetric DKI does not improve precision compared to standard DKI. Furthermore, in the "Single voxel analysis" we have found that without denoising, the tipping point at which the difference between axisymmetric DKI and standard DKI becomes visible typically requires very high SNRs, often above 140. We therefore were interested to see if the tipping point could be reached for realistic SNRs (up to 52) in combination with additional adaptive denoising (msPOAS) with two settings of adaptation parameter λ.[11] The influence of λ was significant for low SNRs while its effect was decreasing the higher the SNR was. We found that for a realistic but high SNR 52, the tipping point was only reached for $\overline{W}$ and $W_{\perp}$ in roughly 1/3 of voxels in the Westin mask if a standard MRI protocol is used and for a high adaptation parameter $\lambda = 100$. In all other cases the number of voxels reaching the tipping point was significantly lower and especially for the diffusion parameters it was close to 0 for realistic SNRs. This indicates that

the bias introduced by the symmetry assumption made in axisymmetric DKI is not going to be visible under realistic, experimental conditions in most of the voxels.

4.5.3 | Quantification of bias in fiber tracts

The noise simulations are more realistic than the noise-free simulation but introduce additional factors that could cause a difference between standard DKI and axisymmetric DKI, for example, model dependent noise susceptibility and the Rician bias. Noisy data was simulated at SNR = 39 and in an earlier study[19] this SNR was found to be sufficient to reduce the difference between both DKI models below 5% in in vivo white matter, see Fig. 6 in Reference 19.

If the noise induced Rician noise bias can be considered negligible if it is below 5% at SNR = 39, the observed difference between axisymmetric DKI and standard DKI estimated for the standard protocol is most likely the axisymmetric DKI inherent bias. Consistent with the findings concerned with the median bias found in Figure 3, the fiber tract analysis, Figure 6, showed that the median bias of the kurtosis AxTM per fiber tract was highest for $W_\perp$, followed by $W_\parallel$ and lowest for $\overline{W}$. Also, both DKI models based on the standard protocol performed very similarly (except for $W_\perp$) which again demonstrates that the tipping point is not reached in most cases under realistic conditions, that is, noise is dominating the bias and not the model differences.

However, some of the findings in the fiber tract analysis were counter-intuitive. In an other study, the corpus callosum was found to predominantly have voxels with a single fiber orientation[36] and could therefore be considered to have less of a complex structure than other tracts making it more likely to fulfill the assumptions made in axisymmetric DKI. However, the corpus callosum had the highest median bias for 2 of 5 AxTM. Furthermore, in Reference 36 the slf tract was reported to host many voxels with two fiber orientations, that is, fiber crossings which would make it prone to failing the assumption of axisymmetric DKI but the slf was one of the tracts with the lowest differences between both DKI models. This finding, again, points to other factors than fiber complexity, here in the form of fiber crossings, playing a role in determining the difference between standard DKI and axisymmetric DKI, as already discussed in Section 4.3.

4.5.4 | Fast "199" protocol versus standard protocol

Axisymmetric DKI's major advantage is its reduced data demand which can save acquisition time if it is used with a fast acquisition protocol. Combination with additional, well known image acceleration techniques like multislice and GRAPPA could speed up acquisition even more. Moreover, the shorter sampling scheme was reported to have better contrast-to-noise ratio compared to standard DKI in rat brains with induced stroke[37] and it is less susceptible to motion artifacts which is even more important in clinical settings than for basic research where the subjects are more used to scanning and thus less probable to move during the acquisition. We set out to investigate potential problems going along with axisymmetric DKI and its assumptions and the fast "199" image acquisition scheme.

For the single voxel analysis, investigating the influence of the MRI protocol on the tipping point revealed that the fast "199" protocol had even higher SNR requirements to reach the tipping point than the standard protocol. This is plausible since reducing the number of diffusion gradients in the MRI protocol makes parameter estimation more prone to the influence of noise because fitting is done with fewer data points. Furthermore, the effective SNR, $\mathrm{SNR}_{\mathrm{eff}} = \mathrm{SNR} \cdot \sqrt{\text{number of } b = 0 \text{ images}}$ is higher for the standard acquisition protocol, since here more and optimally distributed $b = 0$ images are acquired compared to the fast "199" protocol where only one b = 0 image is acquired. In the "white matter Westin mask analysis with adaptive denoising" analysis we found that when switching to the fast "199" measurement protocol, the number of individual voxels that reached the tipping point in total was smaller compared to the standard protocol which is plausible as described above. It is also important to consider that fewer acquired diffusion gradients can go along with disadvantages, for example, FSL's eddy current correction ("eddy") as a preprocessing step will be challenging since it ideally requires to densely sample the whole sphere with the diffusion gradients and a minimum of approximately 10–15 directions for a $b = 1500$ shell with increasing demands for higher shells, see https://fsl.fmrib.ox.ac.uk/fsl/fslwiki/eddy. Note that these requirements do not apply to the eddy current and motion correction algorithm implemented in the ACID toolbox that was used to pre-process the measured dMRI data used for synthetic data generation since here the eddy-current field is estimated independent of the diffusion gradient directions.[38] Furthermore, Rician bias correction depends on an accurate estimate of the noise level σ and the chosen "repeated measures" method (see Section 2.1) works better with more acquired diffusion gradients since it σ is estimated as the SD over the highest diffusion shell. All in all, parameter estimation with the fast "199" protocol is challenged by a higher bias and the baseline difference between both DKI models is likely not visible for realistic SNRs.

5 | CONCLUSION

Axisymmetric DKI offers advantages like a reduced data demand that is relevant in scientific and clinical practice. We asked the question whether these advantages are counteracted by an error related to the intrinsic simplification of the model. We found that in the noise-free case and when using a standard MRI acquisition protocol $D_\perp$, $D_\parallel$, and $\overline{W}$ could be estimated with few SDV with respect to their standard DKI counterpart. For all other parameters, that is, $W_\perp$, $W_\parallel$ and the biophysical parameters, the number of SDV was high. However, the number of SDV can be reduced if a Westin mask is used, suggesting that fiber complexity is one main driver for the differences between both DKI models. Under realistic conditions with noise in the acquired data, the model inherent baseline difference between both DKI variants requires very high SNRs to become visible since it is hidden in the SD otherwise. Furthermore, our results showed that the fast "199" protocol is particularly vulnerable to the effects of noise in the dMRI data but also that adaptive denosing can help counteract these effects. Here, we only contrasted two extreme acquisition protocols, one suited for standard DKI and one optimized for fast axisymmetric DKI. To find the "sweet spot" between noise susceptibility and time reduction in the acquisition protocol a follow-up study is required.

ACKNOWLEDGEMENT

Open Access funding enabled and organized by Projekt DEAL.

FUNDING INFORMATION

This work was supported by the German Research Foundation (DFG Priority Program 2041 "Computational Connectomics", [MO 2397/5-1; MO 2397/5-2], by the Emmy Noether Stipend: (MO 2397/4-1 and MO 2397/4-2) and by the BMBF (01EW1711A and B) in the framework of ERA-NET NEURON.

DATA AVAILABILITY STATEMENT

The open-source ACID toolbox[20] (http://www.diffusiontools.org/) for SPM contains the estimation methods for standard and axisymmetric DKI used in this study (commit hash: 73e1d23dc). Furthermore, a repository hosting the code used for simulation and analysis of the data in this study is available on Github at https://github.com/quantitative-mri-and-in-vivo-histology/apparent_axDKI_differences.

ORCID

Jan Malte Oeschger https://orcid.org/0000-0003-0237-923X

Karsten Tabelow https://orcid.org/0000-0003-1274-9951

Siawoosh Mohammadi https://orcid.org/0000-0003-1311-9636

TWITTER

Siawoosh Mohammadi siawooshmn

REFERENCES

1. Coutu J-P, Chen JJ, Rosas HD, Salat DH. Non-Gaussian water diffusion in aging white matter. *Neurobiol Aging*. 2014;35:1412-1421.
2. Genç E, Fraenz C, Schlüter C, et al. Diffusion markers of dendritic density and arborization in gray matter predict differences in intelligence. *Nat Commun*. 2018;9:1905.
3. Donat CK, Yanez Lopez M, Sastre M, et al. From biomechanics to pathology: predicting axonal injury from patterns of strain after traumatic brain injury. *Brain*. 2021;144:70-91.
4. Zhuo J, Xu S, Proctor JL, et al. Diffusion kurtosis as an in vivo imaging marker for reactive astrogliosis in traumatic brain injury. *Neuroimage*. 2012;59:467-477. Neuroergonomics: The human brain in action and at work.
5. Steven AJ, Zhuo J, Melhem ER. Diffusion kurtosis imaging: an emerging technique for evaluating the microstructural environment of the brain. *Am J Roentgenol*. 2014;202:W26-W33.
6. Taha HT, Chad JA, Chen JJ. DKI enhances the sensitivity and interpretability of age-related DTI patterns in the white matter of UK biobank participants. *Neurobiol Aging*. 2022;115:39-49.
7. Hansen B, Shemesh N, Jespersen SN. Fast imaging of mean, axial and radial diffusion kurtosis. *Neuroimage*. 2016;142:381-393.
8. Hansen B, Khan AR, Shemesh N, et al. White matter biomarkers from fast protocols using axially symmetric diffusion kurtosis imaging. *NMR Biomed*. 2017;30:e3741.
9. Hansen B, Jespersen SN. Recent developments in fast kurtosis imaging. *Front Phys*. 2017;5:40.
10. Hansen B, Lund TE, Sangill R, Jespersen SN. Experimentally and computationally fast method for estimation of a mean kurtosis. *Magn Reson Med*. 2013;69:1754-1760.
11. Tabelow K, Mohammadi S, Weiskopf N, Polzehl J. POAS4SPM: a toolbox for SPM to denoise diffusion MRI data. *Neuroinformatics*. 2015;13:19-29.
12. Tournier J-D, Smith R, Raffelt D, et al. Mrtrix3: a fast, flexible and open software framework for medical image processing and visualisation. *Neuroimage*. 2019;202:116137.
13. Novikov DS, Veraart J, Jelescu IO, Fieremans E. Rotationally-invariant mapping of scalar and orientational metrics of neuronal microstructure with diffusion MRI. *Neuroimage*. 2018;174:518-538.
14. Alexander DC, Dyrby TB, Nilsson M, Zhang H. Imaging brain microstructure with diffusion MRI: practicality and applications. *NMR Biomed*. 2019;32:e3841.
15. Novikov DS, Fieremans E, Jespersen SN, Kiselev VG. Quantifying brain microstructure with diffusion MRI: theory and parameter estimation. *NMR Biomed*. 2019;32:e3998.
16. Becker S, Tabelow K, Voss H, Anwander A, Heidemann R, Polzehl J. Position-orientation adaptive smoothing of diffusion

weighted magnetic resonance data (poas). *Med Image Anal*. 2012;16:1142-1155.
17. Becker S, Tabelow K, Mohammadi S, Weiskopf N, Polzehl J. Adaptive smoothing of multi-shell diffusion weighted magnetic resonance data by mspoas. *Neuroimage*. 2014;95:90-105.
18. Hansen B, Jespersen SN. Data for evaluation of fast kurtosis strategies, b-value optimization and exploration of diffusion MRI contrast. *Sci Data*. 2016;3:160072.
19. Oeschger JM, Tabelow K, Mohammadi S. Axisymmetric diffusion kurtosis imaging with Rician bias correction: a simulation study. *Magn Reson Med*. 2022;89:787-799. doi:10.1002/mrm.29474
20. David G, Fricke B, Oeschger JM, et al. Acid: a comprehensive toolbox for image processing and modeling of brain, spinal cord, and post-mortem diffusion mri data. *bioRxiv*. 2023.
21. André ED, Grinberg F, Farrher E, et al. Influence of noise correction on intra- and inter-subject variability of quantitative metrics in diffusion kurtosis imaging. *PloS One*. 2014;9:1-15.
22. Callaghan MF, Josephs O, Herbst M, Zaitsev M, Todd N, Weiskopf N. An evaluation of prospective motion correction (pmc) for high resolution quantitative mri. *Front Neurosci*. 2015;9:1-9.
23. Tabelow K, Balteau E, Ashburner J, et al. Hmri – a toolbox for quantitative mri in neuroscience and clinical research. *Neuroimage*. 2019;194:191-210.
24. Lätt J, Nilsson M, Wirestam R, et al. Regional values of diffusional kurtosis estimates in the healthy brain. *J Magn Reson Imaging*. 2013;37:610-618.
25. Westin CF, Maier SE, Mamata H, Nabavi A, Jolesz FA, Kikinis R. Processing and visualization for diffusion tensor MRI. *Med Image Anal*. 2002;6:93-108.
26. Fieremans E, Jensen JH, Helpern JA. White matter characterization with diffusional kurtosis imaging. *Neuroimage*. 2011;58:177-188.
27. Tournier JD, Yeh C-H, Calamante F, Cho K-H, Connelly A, Lin C-P. Resolving crossing fibres using constrained spherical deconvolution: validation using diffusion-weighted imaging phantom data. *Neuroimage*. 2008;42:617-625.
28. Veraart J, Nunes D, Rudrapatna U, et al. Noninvasive quantification of axon radii using diffusion MRI. *Elife*. 2020;9:e49855.
29. Manzano-Patron J-P, Moeller S, Andersson JL, Yacoub E, Sotiropoulos SN. Denoising diffusion MRI: considerations and implications for analysis. *Imag Neurosci*. 2023;2:1-29.
30. Hua K, Zhang J, Wakana S, et al. Tract probability maps in stereotaxic spaces: analyses of white matter anatomy and tract-specific quantification. *Neuroimage*. 2008;39:336-347.
31. Jespersen SN, Olesen JL, Hansen B, Shemesh N. Diffusion time dependence of microstructural parameters in fixed spinal cord. *Neuroimage*. 2018;182:329-342.
32. Jelescu IO, Palombo M, Bagnato F, Schilling KG. Challenges for biophysical modeling of microstructure. *J Neurosci Methods*. 2020;344:108861.
33. Schurr R, Mezer AA. The glial framework reveals white matter fiber architecture in human and primate brains. *Science*. 2021;374:762-767.
34. Tabesh A, Jensen JH, Ardekani BA, Helpern JA. Estimation of tensors and tensor-derived measures in diffusional kurtosis imaging. *Magn Reson Med*. 2011;65:823-836.
35. Nørhøj Jespersen S. White matter biomarkers from diffusion MRI. *J Magn Reson*. 2018;291:127-140.
36. Jeurissen B, Leemans A, Tournier J-D, Jones DK, Sijbers J. Investigating the prevalence of complex fiber configurations in white matter tissue with diffusion magnetic resonance imaging. *Hum Brain Mapp*. 2013;34:2747-2766. doi:10.1002/hbm.22099
37. Wu Y, Kim J, Chan S-T, et al. Comparison of image sensitivity between conventional tensor-based and fast diffusion kurtosis imaging protocols in a rodent model of acute ischemic stroke. *NMR Biomed*. 2016;29:625-630. doi:10.1002/nbm.3506
38. Mohammadi S, Möller HE, Kugel H, Müller DK, Deppe M. Correcting eddy current and motion effects by affine whole-brain registrations: evaluation of three-dimensional distortions and comparison with slicewise correction. *Magn Reson Med*. 2010;64:1047-1056.

SUPPORTING INFORMATION

Additional supporting information may be found in the online version of the article at the publisher's website.

Appendix S1. Supporting information: Investigating apparent differences between standard DKI and axisymmetric DKI and its consequences for biophysical parameter estimates.

How to cite this article: Oeschger JM, Tabelow K, Mohammadi S. Investigating apparent differences between standard DKI and axisymmetric DKI and its consequences for biophysical parameter estimates. *Magn Reson Med*. 2024;1-13. doi: 10.1002/mrm.30034